



ELSEVIER

Journal of Alloys and Compounds 297 (2000) 270–281

Journal of  
ALLOYS  
AND COMPOUNDS

www.elsevier.com/locate/jallcom

# In-situ X-ray diffraction study of the decomposition of NaAlH<sub>4</sub>

Karl J. Gross<sup>a,\*</sup>, Steve Guthrie<sup>a</sup>, Satoshi Takara<sup>b</sup>, George Thomas<sup>a</sup><sup>a</sup>Sandia National Laboratories, Livermore, CA 94551-0969, USA<sup>b</sup>Department of Chemistry, University of Hawaii, Honolulu, HI 96822, USA

Received 10 August 1999; accepted 1 September 1999

## Abstract

Phase transitions and crystal structure modifications were observed during the thermal-desorption decomposition of the alanate NaAlH<sub>4</sub>. This was accomplished through the use of in-situ X-ray powder diffraction. A sequence of  $\theta$ - $2\theta$  scans were collected while heating the sample under a vacuum. The resulting diffraction patterns were assembled to provide a *real-time* representation of the decomposition reactions. It was found that upon heating, NaAlH<sub>4</sub> initially experienced a lattice expansion principally in the *c*-axis direction. This was followed by continuous structural distortions observed as erratic variations in the Bragg intensities. Melting of NaAlH<sub>4</sub> was observed at 180°C followed by the rapid precipitation of a cubic Na<sub>3</sub>AlH<sub>x</sub> phase. This phase then underwent a slow transformation into a Na-rich cubic phase. The decomposition of NaAlH<sub>4</sub> doped with a double catalyst (Ti+Zr) was also investigated. The uncatalyzed sample showed no decomposition when held under a vacuum at 150°C for several hours. The catalyzed sample, on the other hand, began to decompose readily into the monoclinic ( $\alpha$ )-Na<sub>3</sub>AlH<sub>6</sub> phase when heated to 100°C in vacuum. At 150°C the ( $\alpha$ )-Na<sub>3</sub>AlH<sub>6</sub> phase decomposed in a second reaction according to  $\alpha$ -Na<sub>3</sub>AlH<sub>6</sub> → 3 NaH + Al + 3/2 H<sub>2</sub>. The two decomposition reactions appear to be interdependent as the second transformation commenced only after the first reaction neared completion. The observed growth of a narrow Al (111) diffraction peak indicates the formation of aluminum crystallites (>100 nm) as a part of the decomposition reactions. This, and the fact that this solid state process is assisted through the interaction of a surface catalyst suggests long-range transport of a metal species. Some mechanisms are proposed to explain the catalytically enhanced kinetics of these materials. © 2000 Elsevier Science S.A. All rights reserved.

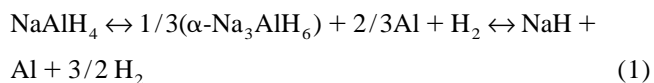
**Keywords:** Metal hydrides; X-ray diffraction; NaAlH<sub>4</sub>; Na<sub>3</sub>AlH<sub>6</sub>; Rietveld refinement

## 1. Introduction

Chemical preparation methods, as well as direct synthesis and decomposition of the compound NaAlH<sub>4</sub> have been developed and described in some detail over the years [1–6]. However, it was the recent work of Bogdanovic and Schwickardi that demonstrated that doping the alkali metal hydride with a TiCl catalyst enabled the ready release and absorption of hydrogen gas [7]. This finding is significant in identifying a new class of hydrides, based on the aluminum hydride complex and non-transition metals, which have potential for use as reversible hydrogen storage media. Prior to this study, it was believed that the slow reaction kinetics at all but high temperatures, made these materials impractical for hydrogen storage. Subsequently Jensen and co-workers found that further kinetic enhance-

ment can be achieved by alternate doping methods [8] and catalysts [9]. The advantage of this class of materials is their high hydrogen weight capacities. NaAlH<sub>4</sub> has a theoretical reversible capacity of 5.5 wt.% H<sub>2</sub>. Other aluminum-hydride complex compounds have even higher theoretical capacities (e.g. Mg(AlH<sub>4</sub>)<sub>2</sub>, 6.95 wt.% H<sub>2</sub>).

These materials are distinct from classical metal hydrides in their structure as well as their properties. Many metal hydrides form through hydrogen occupation of interstitial sites in the host metal lattice. The alanates, however, are formed through complex chemical reactions. In the case of NaAlH<sub>4</sub>, the sorption process involves distinct chemical reactions with the formation of at least one intermediate phase, Na<sub>3</sub>AlH<sub>6</sub>. The reactions in this case are:



We have been investigating NaAlH<sub>4</sub> in depth for two

\*Corresponding author. Tel.: +1-925-294-4639; fax: +1-925-294-3410.

E-mail address: kjgross@sandia.gov (K.J. Gross)

reasons. First of all, with a reversible capacity of 5.5 wt.%  $H_2$ , this compound has merit as a potential storage medium. Secondly, a detailed understanding of the hydriding and dehydriding behavior of this compound will play an important role in the development of improved storage materials based on catalyst assisted complex-based hydrides. Previously we investigated some of the thermodynamic and kinetic properties of this material [10]. Here we will present some results on the investigation of the phase transitions that occur during the thermal decomposition of  $NaAlH_4$ .

Various in-situ X-ray diffraction methods have been described in the literature and have contributed significantly to the fundamental understanding of hydride-forming compounds [11–19]. For example, a special cell was designed by Notten et al. [11], which allowed the simultaneous measurement of hydriding isotherms and X-ray powder diffraction patterns. This system allowed the authors to monitor phase transformations in  $LaNi_5H_x$  during hydrogen absorption and desorption. We have employed a similar arrangement to study the structural changes and phase transformations that occur during the thermal decomposition of  $NaAlH_4$ .

## 2. Sample preparation and experimental details

The material synthesis and catalyst doping were performed in collaboration with and using techniques developed by Jensen and co-workers [8,9]. Sodium aluminum hydride,  $NaAlH_4$ , was obtained both as a solid and as a 1.0 M THF solution from Aldrich Chemical Inc. The material used in these studies was prepared by recrystallizing the solid by adding pentane to a solution of  $NaAlH_4$  in THF or by evaporation of the commercial THF solution to dryness under vacuum. IR spectroscopy performed on these samples indicated that no residual THF was present. The hydride was doped with catalysts using two separate liquid precursors. These were Titanium butoxide  $Ti[O(CH_2)_3CH_3]_4$  and Zirconium propoxide  $Zr[OCH_2CH_2CH_3]_4$  70 wt.% in a 1-propanol solution. Two mole% each of these catalysts were added to about 1.5 g of the dry  $NaAlH_4$  powders. The mixture was then ground together with a mortar and pestle and finally milled in a SPEX<sup>®</sup> mill for 30 s. This process caused a color change in the material from white to dark gray. After doping, about 150 mg of the sample was loaded into the X-ray diffraction cell. All of the above operations, including the loading of the material in the diffraction cell, were performed in an argon glove box ( $<5$  ppm  $O_2$ ) to minimize water and oxygen contamination.

X-ray powder diffraction experiments were performed on a Scintag XDS 2000 diffractometer using  $Cu K_\alpha$  radiation. In-situ measurements were made using a specially designed cell (Fig. 1). Details of the cell construction are given in a schematic drawing shown in Fig. 2. The cell

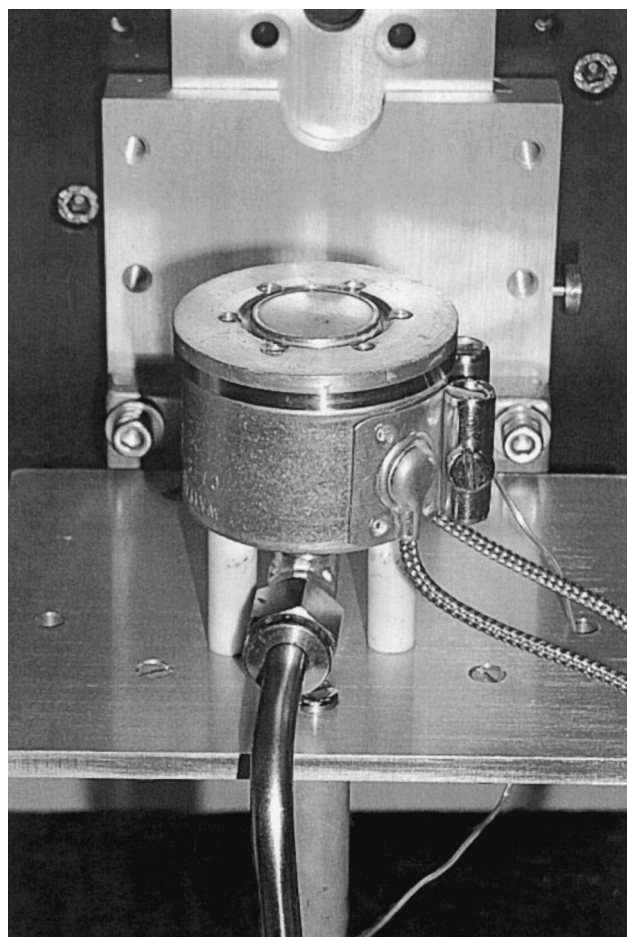


Fig. 1. Photograph of the sample cell used for in-situ X-ray diffraction measurements. The Be window, heating element, and vacuum line are shown.

consisted of a stainless steel CF-40 flange (15 mm ID) to which 4 mm thick aluminum was sinter-bonded. A beryllium disk ( $d=18$  mm, 0.3 mm thick) was welded directly to the aluminum. The beryllium disk acted as an X-ray transparent window and thermal conductor to the sample. The powder sample ( $\sim 150$  mg) was held against the beryllium window by an aluminum disk ( $d=18$  mm, 0.3 mm thick) and a spring. The cell was sealed by another CF-40 flange using sintered-stainless steel-filter copper seals. The backing flange was fitted with a short length of stainless steel tubing to a small valve and a VCR fitting. The samples were loaded and sealed into the cell in an argon glove box. This allowed the samples to be synthesized, prepared and measured without ever exposing them to air. After the cell was loaded, a heating coil was attached and the cell was mounted onto a modified  $z$ -axis stage in the diffractometer. A thermocouple was inserted into a small hole drilled into the cell near the beryllium window. A P.I.D. controller maintained the cell at temperatures up to  $200^\circ C$ . Independent measurements at the beryllium window verified that the sample temperature was within  $\pm 1^\circ C$  of the cell temperature. The cell was con-

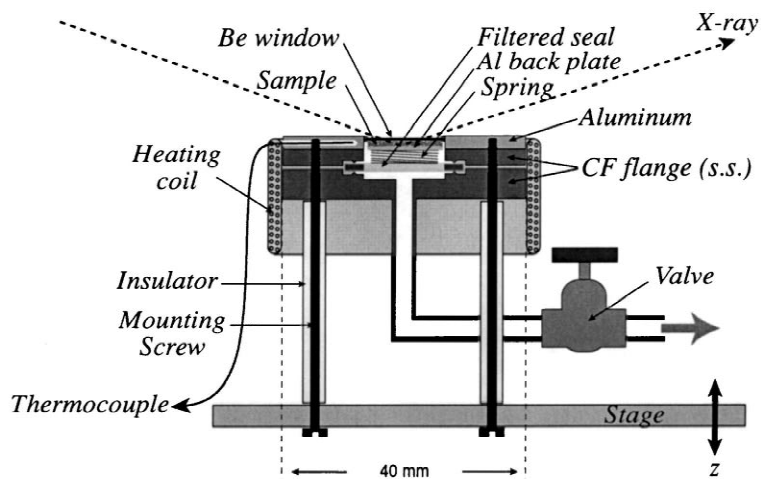


Fig. 2. Schematic diagram of the sample stage used for making in-situ X-ray diffraction measurements.

nected to a manifold which allowed the introduction of argon gas or pumping to a rough vacuum. The manifold was purged several times (argon/vacuum), back-filled with argon, and then the cell's valve was opened. A pressure sensor mounted close to the cell on the transfer line enabled the cell pressure to be monitored.

This particular cell design has several advantages over commercial environmental stages:

1. By holding the sample against the beryllium window, the measuring volume of the sample is maintained in constant Bragg-Brentano focussing conditions.
2. Heating the entire cell, including the beryllium window, ensures better temperature control over the measured volume of the sample.
3. Experiments can be done using samples with high vapor pressures because the cell can be easily cleaned and reused. All of the other internal parts are disposable.
4. The heating elements are external to the cell and are unaffected by reactions that occur within the cell.
5. The cell construction is relatively simple so that the cell can be replaced easily and inexpensively if damaged in an experiment.
6. Control over temperature, pressure and the possibility to add reactive gases or liquids allow for many different types of dynamic investigations. Transitions in crystal structure, phase and chemical composition, as well as solid–liquid or solid–gas phase transitions, can all be observed.

The disadvantages of this system are a temperature limit of about 400°C and the possibility that the sample may react with the beryllium window.

The cell's  $z$ -axis position was first roughly adjusted with a calibration tool. Fine adjustments were made by performing short X-ray diffraction scans and changing the  $z$ -position until the  $\text{NaAlH}_4$  peak positions matched the

literature values. The  $z$ -position changed slightly with heating due to the thermal expansion of the cell material. This causes a  $\cos \theta$  dependent peak shift. Bragg reflections from the beryllium window were used as a calibration standard to correct the data for this effect. The change in going from room temperature to the highest temperature employed (200°C) caused a shift in the Be (100) peak of 0.007°. This shift is small compared to those observed for crystalline deformations and transitions.

Dynamic X-ray diffraction measurements were made by scanning rapidly over a small angle range ( $28.5^\circ \leq 2\theta \leq 40.0^\circ$ ). This angular range was sufficiently broad to capture characteristic peaks of all of the phases involved in the decomposition reactions, while keeping the scan interval to a minimum ( $\Delta t \approx 7$  min). Each peak corresponds to specific crystallographic planes in each of the phases present in the sample. This technique allows one to follow the evolution of individual phases over the course of the experiment. DataScan [20] software was used to make continuous-scan measurements in order to collect the most data in a fixed period of time. Scan rates of  $3^\circ \text{min}^{-1}$  were used with sampling at  $0.02^\circ$ . Up to 250 scans were collected in an individual experiment.

### 3. Results

#### 3.1. Uncatalyzed $\text{NaAlH}_4$

The first set of dynamic in-situ X-ray diffraction measurements were made on an uncatalyzed sample of  $\text{NaAlH}_4$ . In Fig. 3 a sequence of time-resolved  $\theta$ – $2\theta$  scans have been superposed to produce a *real-time* presentation of the phase transformations that occurred when the sample was heated under a vacuum. Sample temperatures are shown along the right hand side of the plot and are correlated with the time of the scans. The following observations can be made from these measurements:

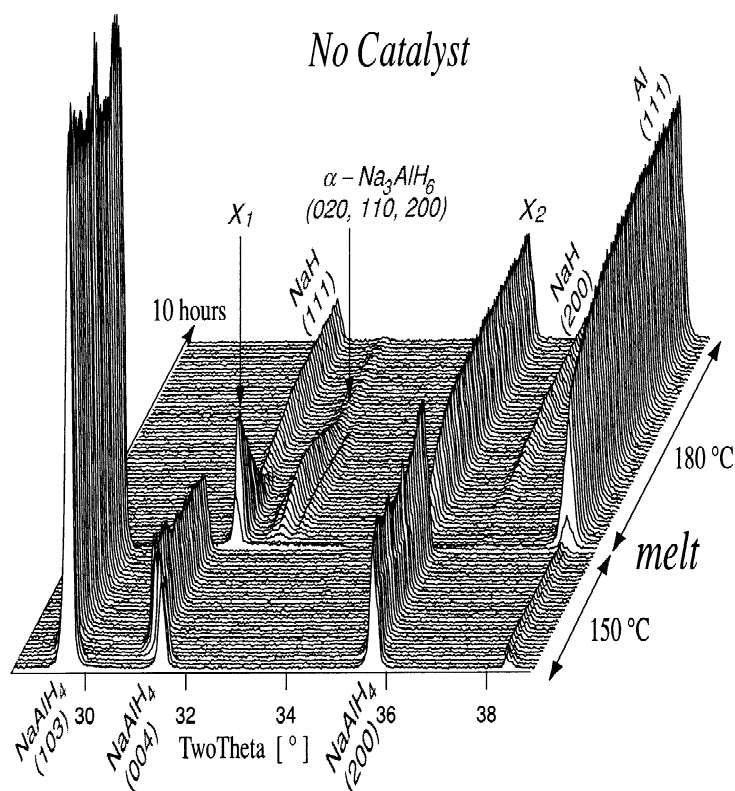


Fig. 3. A series of powder X-ray diffraction patterns taken during the decomposition of uncatalyzed  $\text{NaAlH}_4$ . The sample cell was continuously evacuated and the temperature increased in stages. Melting occurred at  $180 \pm 2^\circ\text{C}$  which can be observed by the abrupt disappearance of the peaks of the  $\text{NaAlH}_4$  phase.

(1)  $\text{NaAlH}_4$  underwent a lattice expansion upon heating.

The lattice parameters of  $\text{NaAlH}_4$  were calculated from a full diffraction pattern taken over a large angle range ( $2^\circ \leq 2\theta \leq 110^\circ$ ) prior to the dynamic measurements. They were determined to be  $a = 5.02654(25) \text{ \AA}$  and  $c = 11.37064(67) \text{ \AA}$ . For the dynamic measurements, an angle range was selected which contained three  $\text{NaAlH}_4$  peaks: (103), (004) and (200). This made it possible to measure the change in the lattice parameters as the sample was heated. The results, which are presented in Fig. 4, show that heating to  $150^\circ\text{C}$  caused an anisotropic lattice expansion of about 1% in the  $c$ -axis direction and about 0.2% expansion in the  $a$ -axis direction.

(2) At  $150^\circ\text{C}$  the  $\text{NaAlH}_4$  peak intensities showed rapid variations over time.

Referring to Figs. 3, 6 and 8 it can be seen that there were relatively rapid and reversible variations in peak intensities of the  $\text{NaAlH}_4$  phase upon heating. This effect does not appear to be due to a decomposition reaction because it was observed in the first part of measurement when no other phases were formed. The changes were also very erratic compared to the changes that occurred in the intensities of the other peaks which formed later in the experiment. These variations are believed to be the result of distortions in the crystal structure of  $\text{NaAlH}_4$ . Since X-rays are fairly insensitive to hydrogen, the changes in

Bragg intensities must be due to motion of the metal atoms. These include displacements, the creation of vacancies or substitutions, and vibrational motions. This behavior indicates high mobility of a metal or metal-hydrogen species within the lattice.

(3) Uncatalyzed  $\text{NaAlH}_4$  showed essentially no desorption at  $150^\circ\text{C}$ .

The areas under each peak in Fig. 3 have been integrated and normalized by each peak's maximum value to give a measure of the relative content of each phase during the experiment. In the case of the  $\text{NaAlH}_4$  phase, the three measured peaks were averaged to smooth out the variations described above. Relative phase contents and sample temperature are plotted versus time in Fig. 5. The  $\text{NaAlH}_4$  and Al contents were essentially unchanged during the first part of the experiment in which the sample was held under vacuum at  $150^\circ\text{C}$  for a period of 4 h. This is consistent with the lack of hydrogen release found during independent isothermal measurements. Thus, the decomposition of uncatalyzed  $\text{NaAlH}_4$  was kinetically hindered under these conditions.

(4)  $\text{NaAlH}_4$  melts above  $180^\circ\text{C}$ .

After holding the sample under a vacuum at  $150^\circ\text{C}$  for 4 h, the temperature was increased to  $180^\circ\text{C}$ . All diffraction peaks associated with the  $\text{NaAlH}_4$  phase abruptly disappeared, indicating a rapid and complete melting of the

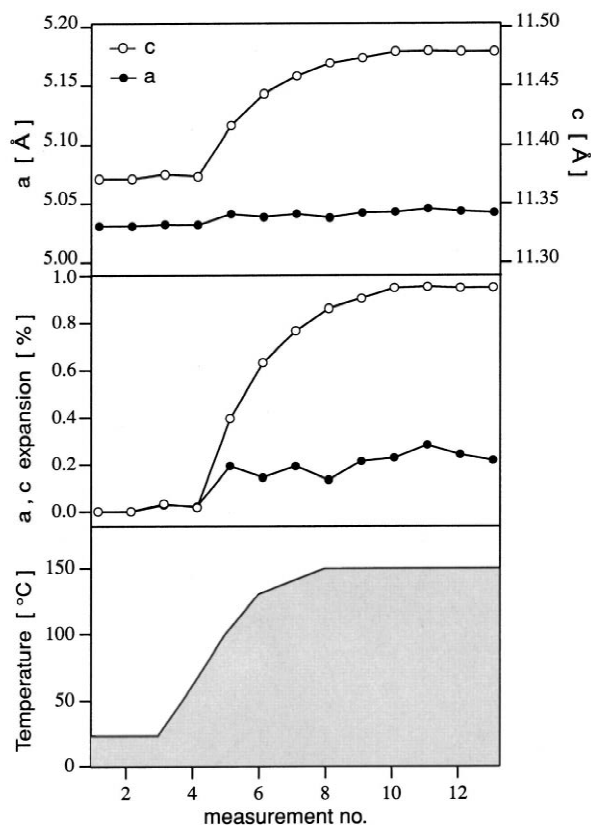


Fig. 4. Changes in the lattice parameters of the monoclinic compound  $\text{NaAlH}_4$  (top) as the sample temperature was increased (bottom). The anisotropy of the lattice expansion is demonstrated in a plot of the percent change in lattice parameters (middle).

sample. This was independently verified by differential scanning calorimetry and is in agreement with previous results [6,1] which reported the melting point to be  $180.8^\circ\text{C}$  and  $183^\circ\text{C}$  respectively.

(5) Phase  $X_1$ : An unidentified phase precipitated immediately from the  $\text{NaAlH}_4$  melt.

Upon melting of the  $\text{NaAlH}_4$ , some hydrogen immediately desorbed and the crystalline Al content of the sample increased rapidly. Since crystalline Al was observed and the hexahydride phase,  $\text{Na}_3\text{AlH}_6$ , is known to have a higher melting temperature, the formation of this intermediate phase was expected as indicated in Eq. (1). However, the formation of a new phase ( $X_1$ ), with a structure different from  $\alpha\text{-Na}_3\text{AlH}_6$ , was observed by the appearance of a peak at  $2\theta = 31.63^\circ$ . This phase precipitated immediately from the melt, and, during two scans, was the only crystalline phase besides aluminum which was present in the sample. The peak intensity from this phase declined fairly rapidly with continued heating. This implies that there was either a structural phase transformation or a chemical decomposition of this phase. A more detailed analysis of this phase is presented later in the discussion.

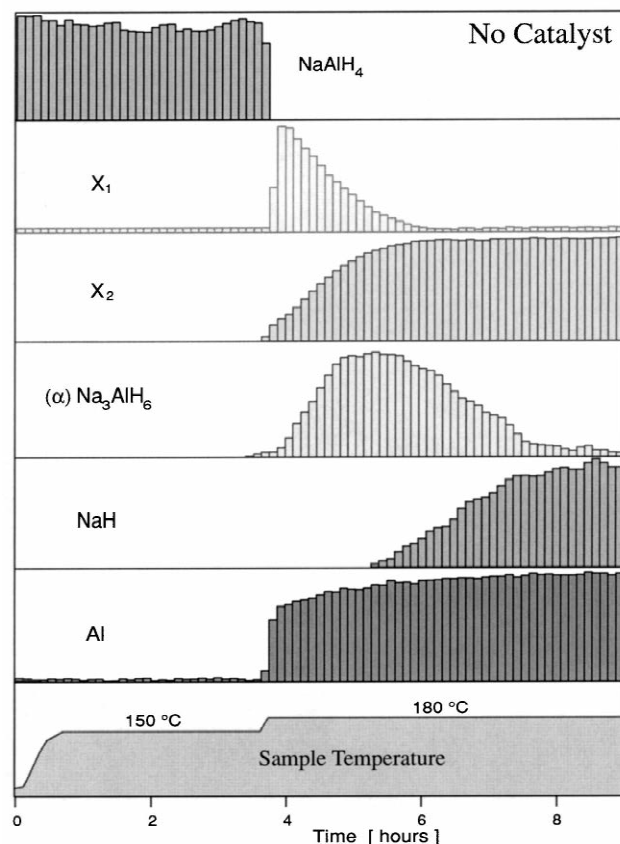


Fig. 5. The integrated intensities of the peaks of each phase present in the series of X-ray diffraction patterns taken during the decomposition of uncatalyzed  $\text{NaAlH}_4$ . These have been normalized to 100% at the maximum concentration of each phase.

(6) Phase  $X_2$ : Peaks from a cubic phase appeared after the melt and grew slowly.

A second unidentified phase ( $X_2$ ) appeared more slowly from the melt and appeared to grow at the same rate as the peak from the previous phase ( $X_1$ ) declined. The formation of this phase may have been due to a chemical interaction with the beryllium window. However, this conclusion stems only from the observation that this phase was not present in a sample which underwent the same process but in a separate autoclave constructed only of stainless steel. A more detailed examination of the crystal structure of this phase is given below.

(7) The monoclinic  $\alpha\text{-Na}_3\text{AlH}_6$  phase formed slowly and then decomposed into  $\text{NaH} + \text{Al}$ .

The (020), (110), and (200) peaks of the monoclinic  $\alpha\text{-Na}_3\text{AlH}_6$  phase began to appear just after the melt at about  $32^\circ$  in the diffraction patterns. This phase grew slowly while the cubic  $X_1$  phase disappeared. When most of the  $\alpha\text{-Na}_3\text{AlH}_6$  phase was formed it began to decompose into  $\text{NaH}$  and  $\text{Al}$ . This was evidenced by the appearance of the  $\text{NaH}$  (111) and (200) peaks as well as a slow increase in the intensity of the  $\text{Al}$  (111) peak. Clearly,

the fact that the  $\alpha$ - $\text{Na}_3\text{AlH}_6$  was observed at all, indicates that its initial decomposition rate was slower than its rate of formation. Eventually, the total amount of  $\alpha$ - $\text{Na}_3\text{AlH}_6$  phase in the sample began to decline. This may be because the formation reaction had reached completion, or simply because the rate of decomposition had overtaken the rate of formation. The latter explanation is very probable since the reaction rates are most likely concentration dependent.

### 3.2. Catalyst Doped $\text{NaAlH}_4$

In-situ X-ray diffraction measurements were performed in the same manner as described above on a sample doped with both the Ti and Zr catalysts. However, in this experiment the temperature was maintained at well below the melting point of  $\text{NaAlH}_4$ . The results of these measurements are shown in Fig. 6 as a sequence of diffraction patterns. Plots of the relative phase content of the sample throughout the desorption process are given in Fig. 7. The following observations can be made:

(1) Catalyst doped  $\text{NaAlH}_4$  decomposed at  $100^\circ\text{C}$ .

An important observation can be made by comparing this experiment with the previous measurements on the uncatalyzed sample. The catalyst doped sample began to decompose immediately at  $100^\circ\text{C}$ , whereas the uncatalyzed

sample showed no signs of decomposition even at  $150^\circ\text{C}$ . Thus, the addition of the catalyst clearly enhanced the kinetics of the  $\text{NaAlH}_4$  -to-  $\alpha$ - $\text{Na}_3\text{AlH}_6$  phase transition.

(2)  $\text{NaAlH}_4$  decomposed into  $\alpha$ - $\text{Na}_3\text{AlH}_6$  and Al.

The  $\alpha$ - $\text{Na}_3\text{AlH}_6$  phase appeared from the start of the decomposition of  $\text{NaAlH}_4$  and grew at a rate comparable to that of the decrease in the  $\text{NaAlH}_4$  content, indicating a phase transition as described by the first reaction of Eq. (1). The sample was held at  $100^\circ\text{C}$  for over 5 h. By this time the decomposition of the  $\text{NaAlH}_4$  phase into the  $\alpha$ - $\text{Na}_3\text{AlH}_6$  phase had slowed to the point that very little change was observed. The temperature was then increased to  $150^\circ\text{C}$ , resulting in a more rapid decomposition rate.

(3) The  $\alpha$ - $\text{Na}_3\text{AlH}_6$  phase decomposed into  $\text{NaH} + \text{Al}$ .

As with the uncatalyzed material, the  $\alpha$ - $\text{Na}_3\text{AlH}_6$  phase decomposed into  $\text{NaH}$  and Al. However, this decomposition reaction did not initiate until the sample temperature was raised to  $150^\circ\text{C}$  and most of the  $\text{NaAlH}_4$  phase was gone. The fact that the  $\alpha$ - $\text{Na}_3\text{AlH}_6$  which was present at  $100^\circ\text{C}$  did not decompose at this temperature gives another indication that the two decomposition reactions of Eq. (1) are interdependent and possibly sequential.

(4) No other phases were formed.

In this experiment no phases other than  $\text{NaAlH}_4$ ,  $\alpha$ - $\text{Na}_3\text{AlH}_6$ ,  $\text{NaH}$ , and Al were observed. The two cubic

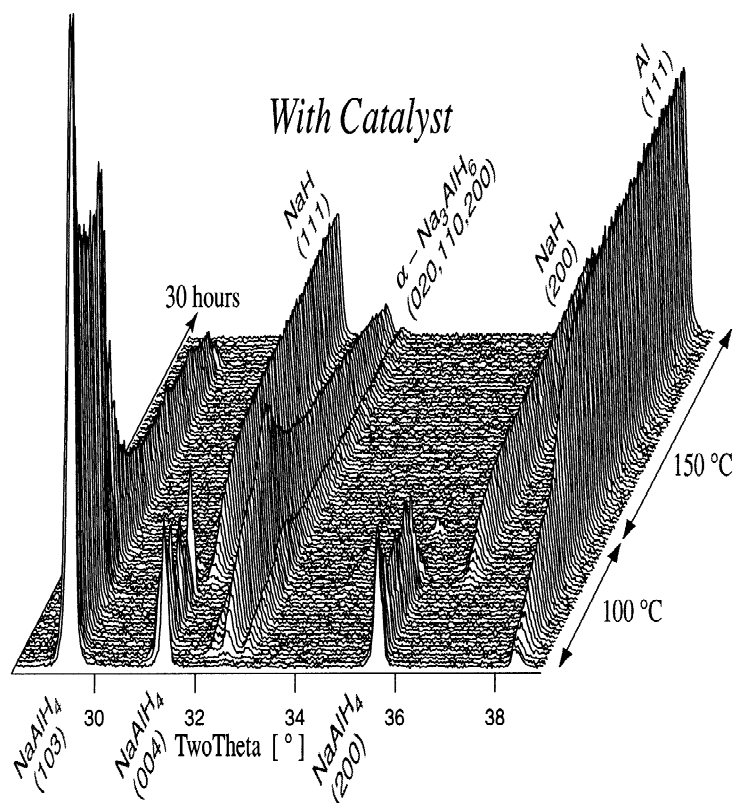


Fig. 6. A series of powder X-ray diffraction patterns taken during the decomposition of  $\text{NaAlH}_4$  doped with a combined Ti and Zr catalyst. The sample cell was continuously evacuated and the temperature increased in stages.

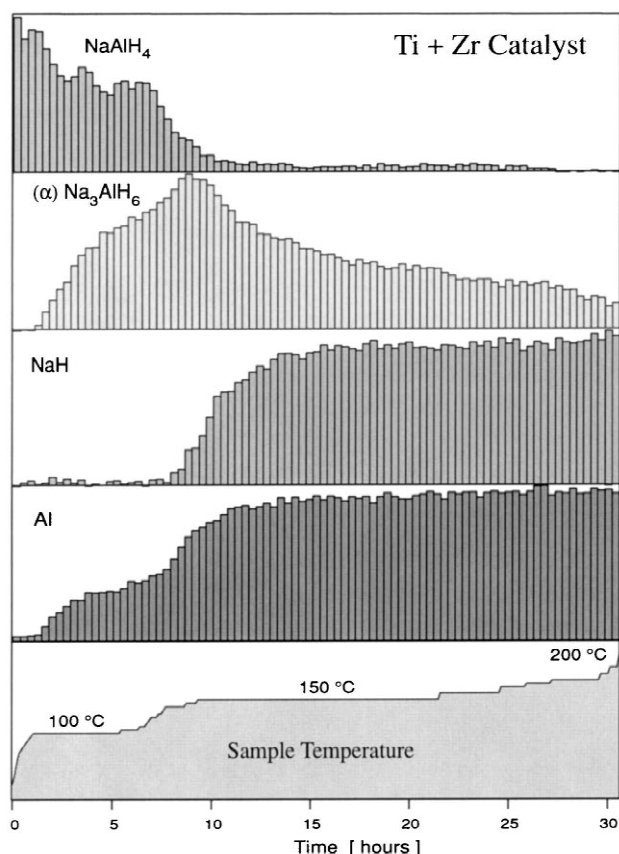


Fig. 7. The integrated intensities of the peaks of each phase present in the series of X-ray diffraction patterns taken during the decomposition of NaAlH<sub>4</sub> doped with a combined Ti and Zr catalyst. These have been normalized to 100% at the maximum concentration of each phase.

phases, “X<sub>1</sub>” and “X<sub>2</sub>”, which were formed in the previous experiment do not appear in any of the present scans.

#### 4. Discussion

Three aspects of this investigation will be discussed. The first is the appearance of two new phases which have not been previously reported. The second is about the formation of crystallites of the reaction products which indicates the transport of metal species during the decomposition reaction. The third issue concerns the reaction mechanisms and the influence of the surface catalyst on bulk behavior. The time-resolved X-ray diffraction experiments demonstrated that the desorption kinetics were dramatically improved by doping the alanate with a Ti/Zr catalyst. However, the role of the catalyst is not clearly understood. We will discuss some possible reaction mechanisms.

##### 4.1. The new phases X<sub>1</sub> and X<sub>2</sub>

Further examination of the two in-situ measurements sheds some light on the two unidentified phases which we

have labeled “X<sub>1</sub>” and “X<sub>2</sub>”. We will first examine the phase labeled X<sub>2</sub>. Its approximate composition can be deduced from a comparison of the two experiments. Assuming that the individual phases crystallize without any preferred orientation, then the absolute intensity of any peak associated with a phase is directly proportional to the quantity of that phase present in the sample. The two experiments can be compared by normalizing the intensities relative to the NaAlH<sub>4</sub> peaks at the start of each experiment. The samples were found to contain the same amount of Al at the end of both experiments. In the second experiment (Figs. 6 and 7) only NaH and Al were present at the conclusion of the experiment, whereas at the end of the first experiment, NaH, Al, and X<sub>2</sub> were all present. Thus, X<sub>2</sub> cannot contain any appreciable amount of aluminum. On the other hand, at the end of the first experiment, when the X<sub>2</sub> phase had reached its maximum concentration, the NaH (111) and (200) peaks had only 1/3 of the intensity of the same peaks at the end of the second experiment. Consequently, X<sub>2</sub> must be composed mostly of Na.

A similar analysis was done for X<sub>1</sub>. In the first experiment (Fig. 3) the X<sub>1</sub> phase precipitated immediately out of the melt, quickly reaching its maximum concentration. Since this phase and aluminum were the only phases present in the sample at this point, X<sub>1</sub> must consist of all of the original Na and whatever Al that has not crystallized as pure aluminum. The crystalline aluminum content of the sample can be found by comparing the intensity of the Al (111) at this point with the intensity of the same peak at the end of the experiment. This, again, is because all of the aluminum at the conclusion of both experiments was found to be in the form of Al metal. The ratio of the peak intensities show that the amount of crystalline aluminum just after the melt was 0.66 of the sample’s total aluminum content. Thus, X<sub>1</sub> must consist of 1/3 of the total Al and all of the Na, or X<sub>1</sub> = 1/3(Na<sub>3</sub>AlH<sub>x</sub>). However, it is not possible to know whether X<sub>1</sub> or X<sub>2</sub> contain hydrogen because of the low scattering cross-section of hydrogen for X-rays. The extended diffraction pattern of the X<sub>1</sub> phase does not agree with published diffraction data of either the α or β phases of Na<sub>3</sub>AlH<sub>6</sub>.

An important aspect of this type of measurement is that interactions and correlations between phases can be observed. The interdependency of X<sub>1</sub> and X<sub>2</sub> becomes apparent when examining the relative phase compositions of Fig. 5. The X<sub>2</sub> content grew at the same rate as X<sub>1</sub> disappeared, and when the X<sub>1</sub> phase was gone, X<sub>2</sub> stopped growing. One can, therefore, conclude that X<sub>2</sub> was a product of the decomposition of X<sub>1</sub>.

To further investigate the phases X<sub>1</sub> and X<sub>2</sub> (in particular their crystal structure) we turn to a third, more detailed, in-situ X-ray diffraction experiment. In this series of measurements the temperature was varied about the melting point of NaAlH<sub>4</sub>, the hydrogen over pressure was manipulated, and a set of full-angle range diffraction

measurements were made during the course of the experiment. An undoped  $\text{NaAlH}_4$  sample was used. The diffraction measurements have been compiled sequentially and are shown in Fig. 8 and the corresponding plot of the relative phase content is given in Fig. 9. Several significant observations can be made directly from these compiled scans. The first is that melting is not necessary for the formation of the  $X_1$  phase. Some of this phase was formed almost immediately on raising the temperature to just below the melting temperature of  $\text{NaAlH}_4$  ( $175^\circ\text{C}$ ). Further along in the experiment, the temperature was briefly raised above the melting point to  $185^\circ\text{C}$  and then lowered to  $150^\circ\text{C}$ . Once again, as in the first experiment in which melting was observed, the intensity of the peak associated with the  $X_1$  phase rose dramatically. In this case, however, peaks from all of the other phases including those of  $\alpha\text{-Na}_3\text{AlH}_6$ ,  $X_2$ , and  $\text{NaH}$  essentially disappeared and the sample's crystalline Al content dropped. The decreasing Al (111) peak intensity can be explained by the consumption of aluminum in the reverse reaction  $X_2$  ( $\text{Na-rich}$ )  $\rightarrow X_1$  ( $\text{Na}_3\text{AlH}_x$ ). Finally the hydrogen over-pressure was raised by shutting the valve to the vacuum pump. This caused the reactions to reverse, consuming the  $X_1$  phase and quickly forming  $\text{Na}_3\text{AlH}_6$  and  $X_2$ . At this elevated temperature the phase transformations  $X_1 \leftrightarrow X_2$  and  $\alpha\text{-Na}_3\text{AlH}_6 \leftrightarrow \text{NaH}$  appear to be highly reversible, driven only by small changes in the hydrogen overpressure. The melting of  $\text{NaAlH}_4$  may play an important role in this behavior, particularly since no catalyst was present.

Another observation from all three measurements is that the decomposition of  $\text{Na}_3\text{AlH}_6$  to  $\text{NaH}$  did not begin at the

first appearance of  $\text{Na}_3\text{AlH}_6$ . In fact,  $\text{NaH}$  only began to form when most of either  $\text{NaAlH}_4$  or  $X_1$  were gone. Thus, these phases must all be interdependent. This was verified in another experiment on uncatalyzed  $\text{NaAlH}_4$ . In that measurement the sample temperature was held constant at  $175^\circ\text{C}$ . The  $X_1$  and the  $\text{Na}_3\text{AlH}_6$  phases grew simultaneously over 5 h. Then the  $X_1$  phase began to transform slowly into  $X_2$ . But it was only after all of the  $X_1$  phase was gone that transformation of  $\text{Na}_3\text{AlH}_6$  into  $\text{NaH}$  was initiated. The fact that these phases all appear to be dependent on each other attest to the notion of some form of long range interactions. This leads to the concept of a highly mobile species responsible for regulating the various decomposition reactions.

The crystal symmetry of the  $X_1$  and  $X_2$  phases were investigated by taking a set of full-angle diffraction patterns just following the melt. A portion of these patterns are included in Fig. 8 and one full pattern is shown in Fig. 10 along with a calculated pattern. This particular diffraction pattern contains the  $X_1$ ,  $X_2$ ,  $\alpha\text{-Na}_3\text{AlH}_6$ , and Al phases, as well as Be from the Be window. The calculated pattern was generated through Rietveld [21] refinements of the data using the program FullProf [22]. Crystal structure parameters (atomic positions, occupancies and thermal parameters), taken from recent neutron diffraction results [23], were input directly for the  $\alpha\text{-Na}_3\text{AlH}_6$  phase. Literature values for the crystal structure of Al were also input directly into the calculations [24]. The fit provides a strong verification of these phases, as well as confirming the lack of any preferred orientation. The cell parameters found for the  $\alpha\text{-Na}_3\text{AlH}_6$  phase were  $a = 5.4536(3) \text{ \AA}$ ,  $b = 5.547(4)$

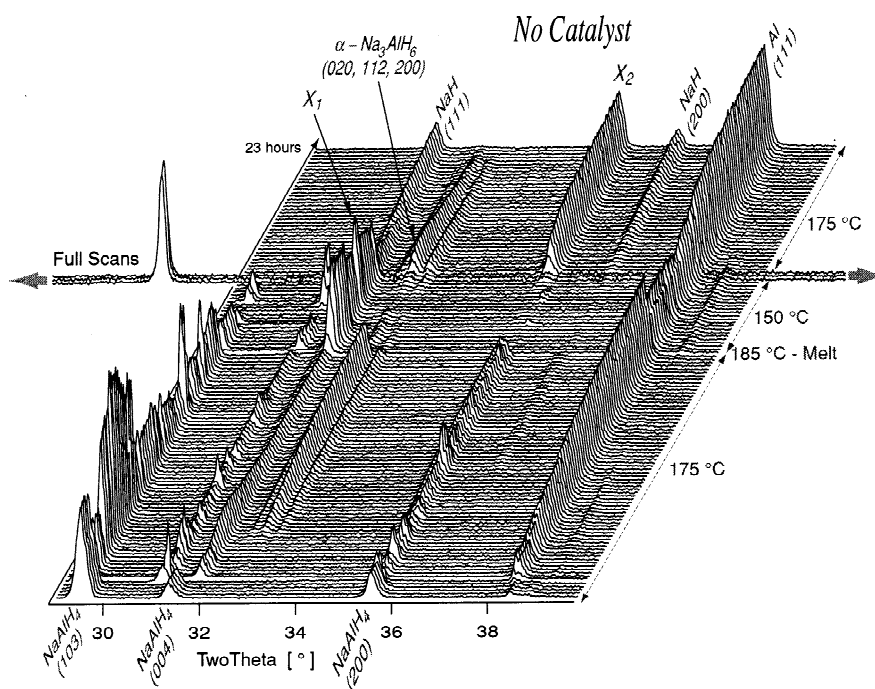


Fig. 8. A series of powder X-ray diffraction patterns taken during the decomposition of uncatalyzed  $\text{NaAlH}_4$ . The sample temperature was held at  $175^\circ\text{C}$  (just below the melting temperature of  $\text{NaAlH}_4$ ) during the initial part of the measurement then increased in stages. A set of full-angle scans was also collected. These are indicated by the arrows.

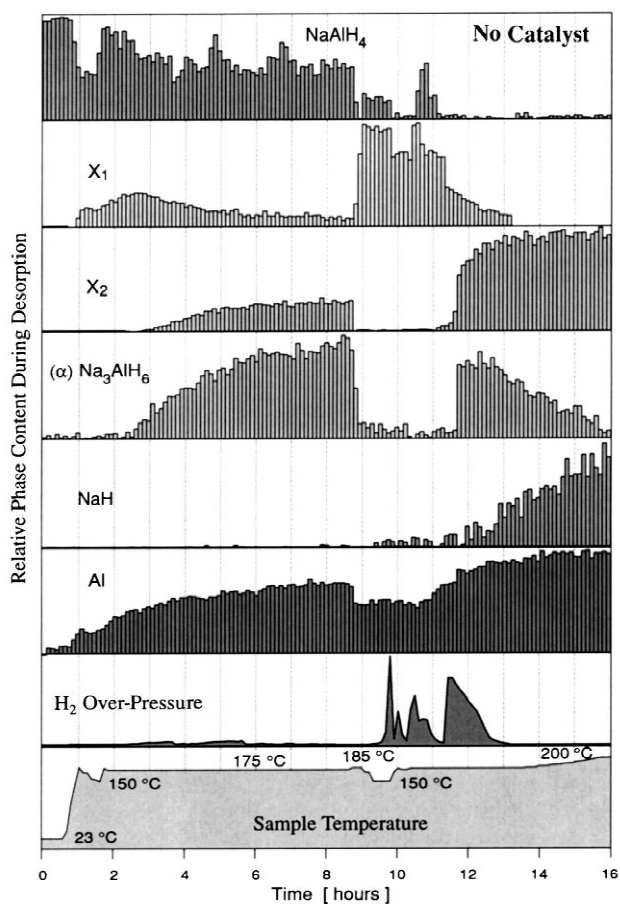


Fig. 9. The integrated intensities of the peaks of each phase present in the series of X-ray diffraction patterns taken during the decomposition of uncatalyzed  $\text{NaAlH}_4$ .

$\text{Å}$ ,  $c = 7.811(4) \text{ Å}$ , and  $\beta = 89.83(7)^\circ$ . For Al the calculated lattice parameter was  $a = 4.0671(5) \text{ Å}$ . These lattice parameters are all about 0.5% larger than the literature values which were measured at room temperature.

PDF (Powder Diffraction Files) database searches provided a basis for choosing the crystal symmetries for the  $X_1$  and  $X_2$  phases [25].  $X_1$  could be described in either the  $Pm-3m$  or  $Immm$  Space Groups, the cubic  $Pm-3m$  symmetry was chosen arbitrarily due to its higher symmetry.  $X_2$  was well characterized by the Space Group  $F-43m$ . This cubic symmetry was confirmed for the  $X_2$  phase in a separate full-angle scan taken at the conclusion of the experiment in which only the  $X_2$ , NaH, and Al phases were present. Pattern matching was employed for the intensities of the  $X_1$  and  $X_2$  phases in the calculated pattern shown in Fig. 10. The lattice parameters were  $a = 7.986(1) \text{ Å}$  for the  $X_1$  ( $Pm-3m$ ) phase and  $a = 7.182(1) \text{ Å}$  for the  $X_2$  ( $F-43m$ ) phase. The resulting peak positions and intensities are presented in Table 1 for  $X_1$  and Table 2 for  $X_2$ . No known crystal structure was found that described either phase. In particular, the most obvious candidate for  $X_1$  is the high-temperature  $\beta\text{-Na}_3\text{AlH}_6$  phase. This phase is cubic and has the same basic

$\text{Na}_3\text{AlH}_x$  stoichiometry. It was previously described in the literature as a metastable phase resulting from a polymorphic transition analogous to that which occurs in the Fluoride Cryolite [26]. However, the reported peaks do not match those of the  $X_1$  phase. The crystal structure of Cryolite and its polymorphic transition has been investigated in great depth [27], but, application of the orthorhombic ( $Immm$ ) structure of the  $\beta$ -phase Cryolite and variations of this structure proved unsatisfactory in reproducing the diffraction pattern measured for the  $X_1$  phase. However, it is still reasonable to believe that there is some correspondence between the two systems in that it is likely that the  $X_1$  phase is indeed the high-symmetry polymorph of  $\alpha\text{-Na}_3\text{AlH}_6$  phase. Single-crystal and neutron diffraction measurements are needed to resolve the structure of this and the  $X_2$  phase.

#### 4.2. Transport of metal species

Because the phase transitions of Eq. (1) occur through rapid solid-state decomposition reactions, one would expect that they take place locally. Thus, after decomposition, the resulting material ought to be a rather homogeneous mixture composed of extremely small domains of each phase. However, this was not the case. The in-situ diffraction experiments showed narrow peaks for each product phase, indicating that these phases were actually present as relatively large crystallites ( $>100 \text{ nm}$ ). This, in turn, implies that there must be some long-range mechanism transporting metal species to the sites where the crystallites are formed.

For example, the formation of crystalline Al was observed as a product of each of the decomposition reactions. Thus, in the decomposition of both  $\text{NaAlH}_4$  and  $\alpha\text{-Na}_3\text{AlH}_6$ , Al must be transported towards (or Na away from) the growing Al crystallites. How this transport occurs and what role the catalyst plays is not known at this point. There are a host of potential transport mechanisms and diffusing species. Some possible diffusing species are  $\text{AlH}_3$  and NaH molecules or  $\text{Na}^-$ ,  $\text{Al}^{3-}$ , Al–H and  $\text{H}^+$  ions, and perhaps even the catalysts. Whatever the diffusing species are, they must be highly mobile in order to achieve the relatively rapid solid-state reactions that are observed.

#### 4.3. Decomposition mechanisms

Another unusual aspect of these materials concerns the catalytic process. Having done quantitative Auger spectra analysis, we know that most of the catalyst remains on the sample's surface [28]. How a surface catalyst can effect a solid-state chemical transition of the entire bulk is not fully understood.

Some reaction mechanisms can now be considered, based on the indications of long-range transport of metal

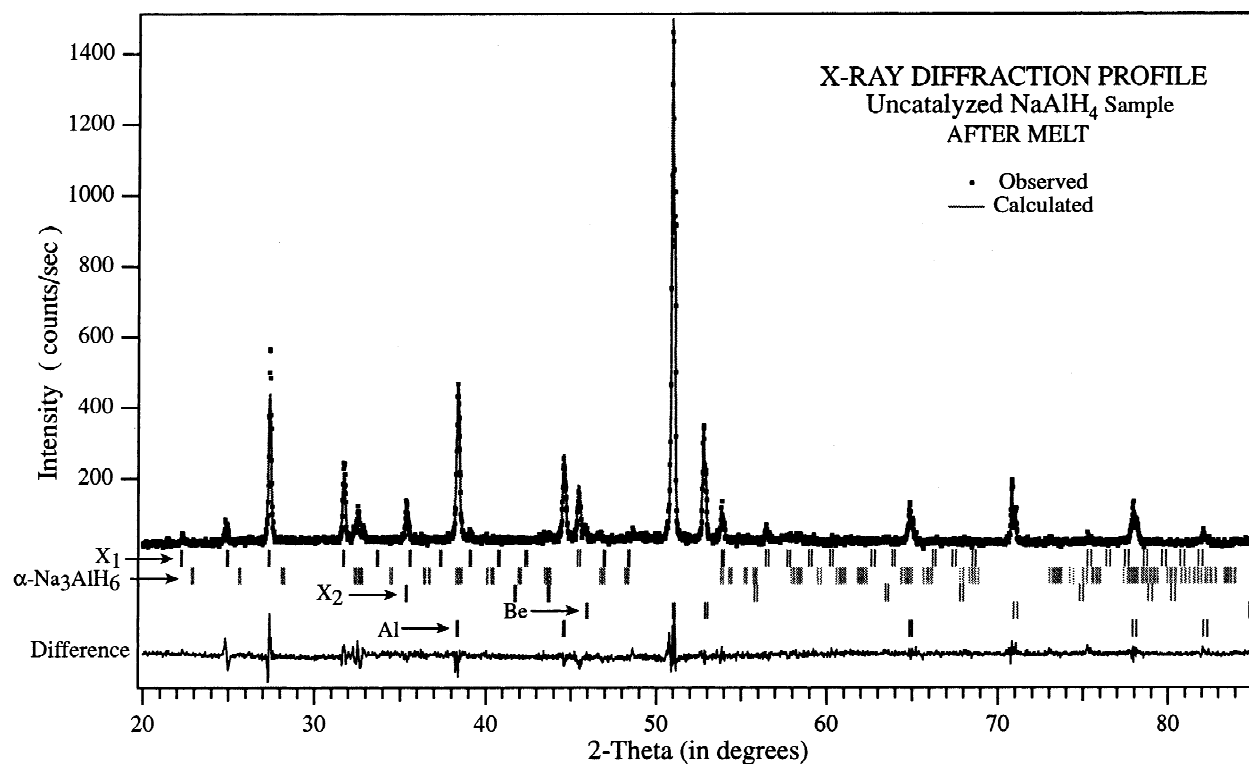


Fig. 10. Rietveld pattern matching of uncatalyzed  $\text{NaAlH}_4$  taken shortly after melting. Shown are calculated fits for the cubic  $X_1$ , monoclinic  $\alpha\text{-Na}_3\text{AlH}_6$ , Al, Be and a cubic  $X_2$  phase.

Table 1

Observed and calculated intensities for the cubic  $Pm\text{-}3m$   $\text{Na}_3\text{AlH}_x$  phase  $X_1$ , calculated intensities were derived from pattern-matching mode only

$h$	$k$	$l$	Mult	$2\theta$ ( $^\circ$ )	$d$ ( $\text{\AA}$ )	$I_{\text{calc}}$ (%)	$I_{\text{obs}}$ (%)
2	0	0	3	22.270	3.98859	0.7	0.7
2	1	0	6	24.939	3.56744	1.2	1.2
2	1	1	12	27.363	3.25667	19.0	19.3
2	2	0	6	31.699	2.82039	8.9	9.0
3	0	0	3	33.678	2.65904	0.1	0.1
3	1	1	12	37.357	2.40519	0.2	0.2
2	2	2	12	39.084	2.3028	3.4	3.5
4	0	0	2	45.442	1.99429	5.7	5.8
3	3	0	12	48.368	1.88026	0.1	0.1
4	2	2	12	56.465	1.62833	1.9	1.9
5	0	0	2	57.737	1.59544	0.1	0.1
4	4	0	6	66.217	1.41019	0.3	0.3
5	4	1	12	77.479	1.23091	0.1	0.1

Table 2

Observed and calculated intensities for the cubic  $F\text{-}43m$  Na-rich phase  $X_2$ , calculated intensities were derived from pattern-matching mode only

$h$	$k$	$l$	Mult	$2\theta$ ( $^\circ$ )	$d$ ( $\text{\AA}$ )	$I_{\text{calc}}$ (%)	$I_{\text{obs}}$ (%)
1	1	1	8	21.413	4.146	0.4	2.31
2	2	0	12	35.321	2.539	16.4	6.06
2	2	2	8	43.624	2.073	2.0	3.05
4	2	2	24	63.399	1.466	1.4	3.09

species and the influence of a surface catalyst on bulk transitions. Three possibilities are:

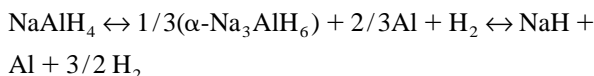
The phase transformations of Eq. (1) occur by the long-range diffusion of metal species through the alanates to the catalyst. The  $\text{NaAlH}_4 \rightarrow \text{Na}_3\text{AlH}_6$  phase transition (and possibly  $\text{Na}_3\text{AlH}_6 \rightarrow \text{NaH}$ ) take place in the bulk by a local restructuring caused by the depletion of Al (or increase in Na). Hydrogen is released and Al crystallites form at the surface through the influence of the catalyst.

There is a complete phase separation throughout the bulk caused by catalytically enhanced hydrogen desorption. The product phases are precipitated through the long-range transport of metal species. The catalyst acts as a hydrogen dissociation–recombination site and possibly also a nucleation site for other phases.

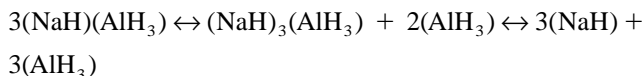
The catalyst itself migrates through the bulk stimulating phase separation and crystal growth.

We will examine the first concept by exploring some hypothetical transport mechanisms. The alanates are viewed as salts of  $\text{AlH}_4^+$  complexes ionically bound to  $\text{Na}^-$ , it is possible that Al or Na is liberated from the surface or migrates in the bulk as  $\text{AlH}_4^+$ ,  $\text{Na}^-$ , other ionic or molecular species. The high mobility of such species would allow for the transport of Al to (or Na away from) sites where the nucleation and growth of Al crystallites occurs. The transport mechanism itself may be diffusion or sublimation and redeposition. At this point no particular transport species has been identified. However, as an

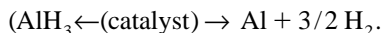
example the transport of molecular NaH or  $\text{AlH}_3$  can be examined. Eq. (1):



can be artificially reformulating to reflect such a transport and dissociation process:



where



In this example, the observed phase transitions are caused by the transport of molecular NaH or  $\text{AlH}_3$ . Furthermore,  $\text{AlH}_3$  molecules would dissociate at the catalyst into Al and  $\text{H}_2$ . Regardless of what species is being transported some support for this model comes from the fact that  $\text{NaAlH}_4$  can be synthesized indirectly by mixing  $\text{Na}_3\text{AlH}_6$  [3] or NaH [1] with  $\text{AlH}_3$  in a solution of Tetrahydrofuran.

The crystal structures of the  $\text{NaAlH}_4$  and  $\alpha\text{-Na}_3\text{AlH}_6$  phases accommodate the notion of bulk transport of a metal species. Ball-and-stick representations of the structures of  $\text{NaAlH}_4$  [29] and  $\text{Na}_3\text{AlH}_6$  [23] are shown in Figs. 11 and 12 respectively. When viewed from the appropriate direction, the alanates are seen to consist of an array of columns of  $\text{AlH}_4^+$  complexes and columns of  $\text{Na}^-$  ions.

Expanding on the concept that the phase transitions occur in the bulk by a local restructuring, facilitated through diffusion, we will give one example of how  $\text{NaAlH}_4$  might transform into  $\text{Na}_3\text{AlH}_6$  (plus Al and  $\text{H}_2$ ) via crystal restructuring. For simplicity, this is depicted as a systematic restructuring in the schematic representation of Fig. 13. The transformation can be achieved by removing an Al and three H's from two out of every three  $\text{AlH}_4^+$  complexes in the double columns at the surface (possibly

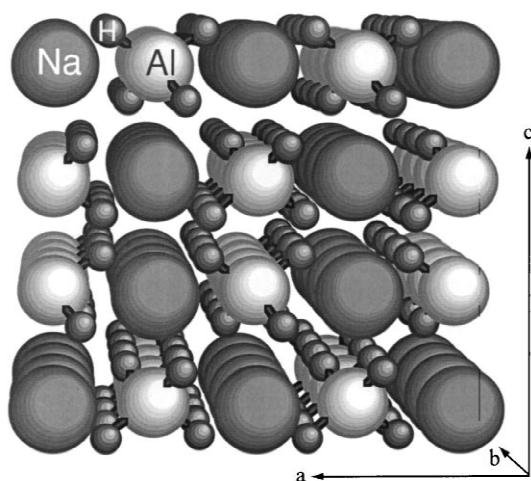


Fig. 11. A ball-and-stick representation of the crystal structure of  $\text{NaAlH}_4$ .

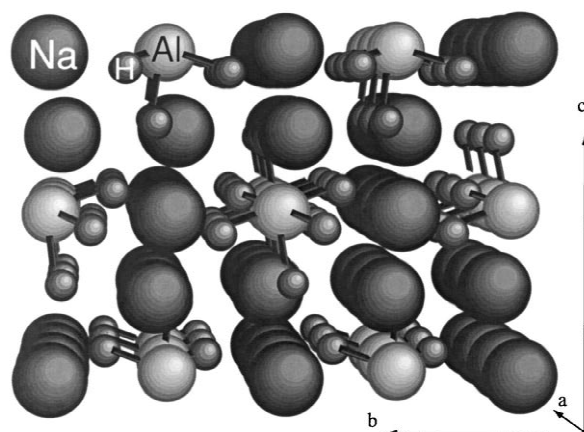


Fig. 12. A ball-and-stick representation of the crystal structure of  $\alpha\text{-Na}_3\text{AlH}_6$ .

by volatilizing  $\text{AlH}_3$  molecules). Filling the vacancy left by the Al with the Na atom closest to it will reproduce the  $\text{Na}_3\text{AlH}_6$  structure in the first monolayer at the surface. For this structural change to propagate into the bulk, the remaining Al and three H's at the surface must be removed and replaced by an Al and three H's from the  $\text{AlH}_4^+$  complex in the column behind it. The catalyst can be pictured as breaking Al–H bonds at the surface to form  $\text{H}_2$  molecules which are liberated as a gas. At the same time atomic Al coalesce to form Al crystallites. In this model the reversible, structural and compositional phase transition can be viewed as a ‘zippering’ of (Al + 3 H) in and out of the double chains of  $\text{AlH}_4^+$  complexes in the bulk. Through this mechanism the catalyst can promote the decomposition/reformation reactions while remaining fixed at the surface.

The second possible reaction mechanism pointed out above is a complete phase separation throughout the bulk caused by catalytically enhanced hydrogen desorption. In this case, atom hydrogen would diffuse through the bulk to the surface where the catalyst acts to recombine it into molecular hydrogen which is then desorbed. The release of hydrogen from the  $\text{AlH}_4^+$  complex would destabilize the alanates. The product phases then precipitate from the

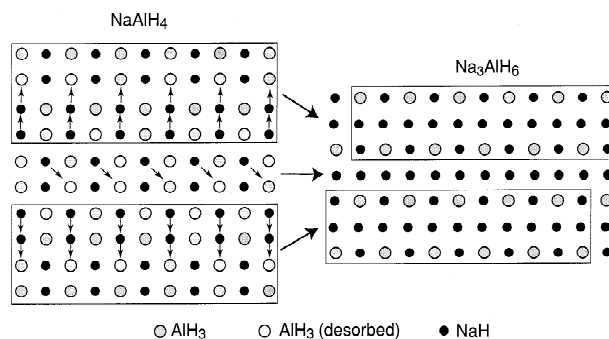


Fig. 13. A schematic representation of a possible mechanism for the crystal structure transformation of  $\text{NaAlH}_4$  to  $\alpha\text{-Na}_3\text{AlH}_6$ .

decomposed alanates through long-range transport of metal species.

The third possible reaction mechanism mentioned earlier was the transport of the catalyst with the reaction boundary as it moves into the bulk. Simply put, in the decomposition reactions, the starting phases ( $\text{NaAlH}_4$  or  $\text{Na}_3\text{AlH}_6$ ) would be consumed and the product phases formed at the catalyst as it 'eats' its way through the material. The reverse reactions are somewhat more difficult to imagine without some transport of the reactant species. Otherwise, all of the solid-phase reactants would have to be simultaneously in contact with the catalyst for the formation reaction to proceed.

## 5. Conclusion

This study focused on understanding the structural and phenomenological properties related to the thermal desorption of hydrogen from  $\text{NaAlH}_4$ . Above  $180^\circ\text{C}$ , the melting of  $\text{NaAlH}_4$  invoked a series of decomposition reactions involving transitions from a cubic  $\text{Na}_3\text{AlH}_x$  phase to a cubic Na-rich phase, as well as the formation of monoclinic  $\alpha\text{-Na}_3\text{AlH}_6$  which decomposed further into NaH. Enhanced desorption kinetics were clearly demonstrated for  $\text{NaAlH}_4$  doped with a double Ti and Zr catalyst. In-situ X-ray diffraction is a unique tool that allows the observation of the growth and decay of individual phases in complex reactions. This technique has helped to provide a deeper understanding of the hydrogen desorption behavior of  $\text{NaAlH}_4$ .

## Acknowledgements

Funding for this project is provided by the U.S. Department of Energy, Office of Power Technologies, Hydrogen Program Office under contract No. DE-AC36-83CH10093. The authors wish to acknowledge the many helpful discussions of G. Sandrock, operating agent for IEA Task 12. Special thanks go to Don Meeker for sample preparation and technical support.

## References

- [1] A. E. Finholt, G.D. Barbaras, G.K. Barbaras, G. Urry, T. Wartik, H.I. Schlesinger, *J. Inorg. Nucl. Chem.* 1 (1955) 317.
- [2] E.C. Ashby, P. Kobetz, *Inorg. Chem.* 5 (9) (1966) 1615.
- [3] M. Mamula, T. Hanslík, *Coll. Czechoslov. Chem. Commun.* 32 (1967) 884.
- [4] T.N. Dymova, N.G. Eliseeva, S.I. Bakum, Yu.M. Dergachev, *Dokl. Akad. Nauk SSSR* 215 (1974) 1369, Engl. 256.
- [5] T.N. Dymova, Yu.M. Dergachev, V.A. Sokolov, N.A. Grechanaya, *Dokl. Akad. Nauk SSSR* 224 (3) (1975) 591.
- [6] P. Claudy, B. Bonnetot, G. Chahine, J.M. Letoffe, *Thermochim. Acta* 38 (1980) 75.
- [7] B. Bogdanovic, M. Schwickardi, *J. Alloys Comp.* 253 (1997) 1.
- [8] C.M. Jensen, R.A. Zidan, N. Mariels, A.G. Hee, C. Hagen, *Int. J. Hydrogen Energy* 24 (5) (1999) 461.
- [9] R.A. Zidan, S. Takara, A.G. Hee, C.M. Jensen, *J. Alloys Comp.* 285 (1999) 119.
- [10] G.J. Thomas, S.E. Guthrie, K.J. Gross, in: *Proceedings 1999 DOE Hydrogen Program Technical Peer Review*, 1999.
- [11] P.H.L. Notten, J.L.C. Daams, A.E.M. De Veirman, A.A. Staals, *J. Alloys Comp.* 209 (1994) 85.
- [12] F.A. Kuijpers, *Philips J. Res. Repts. Suppl.*, No. 2 (1973).
- [13] H.H. van Mal, *Philips J. Res. Repts. Suppl.*, No. 1 (1976).
- [14] J.J.G. Willems, *Philips J. Res. Suppl.* 39 (1) (1984) 1.
- [15] N. Gerard, *J. Phys. E* 7 (1974) 509.
- [16] S. Ono, K. Normura, E. Akiba, H. Uruno, *J. Less-Common Met.* 113 (1985) 113.
- [17] G.J. Gainsford, L.D. Calvert, J.J. Murray, J.B. Taylor, *Proc. Adv. X-ray Analyses* 26 (1983) 163.
- [18] D.G. Ivey, D.D. Northwood, *Scr. Metall.* 19 (1985) 1319.
- [19] T. Hirata, T. Matsumoto, M. Amarro, Y. Sasaki, *J. Phys.* 11 (1981) 251.
- [20] DataScan, MDI Inc., Livermore, CA
- [21] H.M. Rietveld, *J. Appl. Cryst.* 2 (1969) 65.
- [22] J. Rodriguez-Carvajal, *Physica B* 192 (1993) 55.
- [23] E. Rönnebro, Ph.D. Thesis, Stockholm University, 1999.
- [24] P. Villars, L.D. Calvert (Eds.), *Pearson's Handbook of Crystallographic Data for Intermetallic Phases*, Amer. Soc. for Metals, 1985, p. 894.
- [25] Powder Diffraction File, Inorganic volume, JCPDS International Center for Diffraction Data (1997).
- [26] J.P. Bastide, B. Bonnetot, J.M. Letoffe, P. Claudy, *Mat. Res. Bull.* 16 (1981) 91.
- [27] H. Yang, S. Ghos, D.M. Hatch, *Phys. Chem. Minerals* 19 (1993) 528.
- [28] M.W. Clift, personal communication.
- [29] B.M. Bell'skii, A.V. Bulychev, A.V. Golubeva, *Russian J. Inorg. Chem.* 28:10 (1983) 1528.